Small angle X-ray scattering study of pre-nucleation behavior of titanium-free and titanium-bearing diopside glasses

Lung-Chuan Kuo and R. James Kirkpatrick

Department of Geology, University of Illinois
Urbana, Illinois 61801

Abstract

The kinetics of nucleation in titanium-bearing and titanium-free diopside glasses has been studied at small undercoolings. Small angle X-ray scattering (SAXS) techniques have been used to determine the concentration and size of nuclei with radii less than the critical radius in these glasses. Results of the SAXS analysis indicate that the radius of gyration (a measure of the average radius) of the subcritical nuclei ranges from about 200 to 650Å, and increases with increasing time for each composition at each undercooling and with increasing TiO_2 content at a given time and undercooling. The number of subcritical nuclei (1.3×10^1 to 6.8×10^3 cm^{-3}) increases more rapidly than linearly at each undercooling and TiO_2 content and exhibits a trend similar to that of ordinary transient nucleation density variation. The long time (approaching steady state) rate of increase in number of these nuclei (42.1 to 137 cm^{-3} hr^{-1}) increases linearly with increasing TiO_2 content, while the "induction time" (10 to 47 hours) decreases with increasing TiO_2 content at both undercoolings. These data are qualitatively consistent with the traditional physical picture of transient nucleation and yield a melt-crystal surface energy of the order of a few hundred ergs/cm^2. The non-steady state behavior can be described by the theory of transient nucleation developed by Kaschiev (1969).

Introduction

The crystallization of a silicate melt occurs by the formation of a small volume of crystal in the melt (nucleation) and the increase in size of these nuclei (crystal growth). Although there have been a number of recent theoretical and experimental investigations of nucleation and growth kinetics in geologically important systems (see Lofgren, 1980; Kirkpatrick, 1981, for reviews), nucleation, particularly at small undercoolings, is very poorly understood. The major experimental problems are that nucleation at small undercoolings is often sluggish, and that the nuclei are submicroscopic, so that quantitative data on nucleation kinetics are difficult to collect. It is also not possible to reheat the samples at a lower temperature to grow the nuclei to a small but microscopically visible size without more nucleation taking place at that temperature. Thus, methods of study other than direct microscopic observation are desired.

One method to determine the average size and shape of small heterogeneities between about 10Å and a micron in size is small angle X-ray scattering (SAXS). This method has been widely applied to phase separation studies in materials science (Gerold and Kostorz, 1978), metallurgy (Gerold, 1967), biology (Kratky, 1963), and many other fields (Hosemann *et al.*, 1970). Particle sizes in various phase-separated silicate glasses have been determined using this method (*e.g.*, Williams *et al.*, 1965; Hench *et al.*, 1971; Neilson, 1972; Patel *et al.*, 1972; Faber and Rindone, 1980).

The purpose of this study is to investigate the nucleation kinetics in diopside composition melt as a function of temperature and titanium content at small undercoolings. The number and radius of gyration of subcritical nuclei are calculated from SAXS analysis and the rate of increase in number of subcritical nuclei is determined. These results are interpreted in terms of nucleation theory and silicate melt structure.

Theory of SAXS

Detailed treatment of the theory of SAXS has been given by Guinier and Fournet (1955) and Hosemann *et al.* (1970). Several concise reviews of the theoretical and experimental aspects of SAXS are also available (*e.g.*, Guinier, 1963; Kratky, 1963; Ger-

old, 1967; Gould, 1971). In this section only the theory of SAXS pertaining to the present study is outlined.

For a system in which identical, widely dispersed particles of volume v_p, and uniform electron density ρ, are suspended in a matrix of electron density ρ', the intensity of X-rays scattered at small angles can be written

$$I(\varepsilon) = n^2 \exp\left(-\frac{4\pi^2 R_g^2}{3\lambda^2} \varepsilon^2\right), \qquad (1)$$

where ε is the scattering angle, λ is the wavelength of the incident X-ray, R_g is the radius of gyration of the particles, $n^2 = v_p^2 (\Delta\rho)^2 I_e N_p$, I_e is the intensity scattered by one electron, $\Delta\rho = \rho - \rho'$, and N_p is the number of particles per unit volume (Guinier, 1963). Thus, a plot of log I vs. ε^2 (referred to as the Guinier plot) tends to yield a straight line of slope α for small values of ε:

$$\alpha = \frac{4\pi^2}{3\lambda^2} 0.4343 R_g^2. \qquad (2)$$

For CuKα radiation

$$R_g = 0.644 (-\alpha)^{1/2} \text{ Å}. \qquad (3)$$

If there is a distribution of sizes of geometrically similar particles the measured radius of gyration is given by the relationship

$$R_g^2 = \frac{\sum_k p_k R_{gk}^8}{\sum_k p_k R_{gk}^6} \qquad (4)$$

(Guinier and Fournet, 1955). Thus the radius of gyration is heavily weighted towards the larger sizes. In fact, Guinier and Fournet (1955) have shown that at very small angles, where the data of this work have been collected (see below), the scattering intensity is dominated by only the largest particles. Thus, the radius of gyration determined from our measurements is likely to be a good measure of that of the largest particles.

Another important factor is the integrated intensity of the scattered beam, Q, given by

$$Q = 4\pi \int_0^\infty s^2 I(s) \, ds = I_e(\Delta\rho)^2 V c(1 - c) \Theta \qquad (5)$$

(Guinier and Fournet, 1955; Patel *et al.*, 1972), where $\Theta = \exp(-\mu_m\rho_m l)$, V is the volume of sample, c is the volume fraction occupied by the particles, Θ is the transmissivity of the samples, μ_m is the X-ray mass absorption coefficient, ρ_m is the mass density of the sample, and l is the thickness of the sample. The value of c may be determined if Q, I_e and $(\Delta\rho)^2$ can be evaluated. The number of particles per unit volume is given by

$$N_p = c/v_p \qquad (6)$$

(Gerold, 1967).

Experimental procedure

The starting materials used in this study were prepared from reagent grade $CaCO_3$, MgO (Mallinckrodt Inc.) and TiO_2 (Baker Co.) and ultrapure SiO_2 (Johnson Matthey Co. and Aldrich Co.). Homogeneous mixtures of appropriate amounts of each powder were fired to drive out CO_2 and then melted in a Pt crucible in a Deltech $MoSi_2$ resistance furnace at about 1470° C for 2 to 5 hours. The resulting glass was reground and remelted twice. Three compositions were made: Pure diopside, diopside + 0.5 wt.% TiO_2, and diopside + 1.0 wt.% TiO_2.

Isothermal experiments at atmospheric pressure were carried out at undercoolings from 10° to 50° C. Each run consisted of about 5 g of glass in a Pt foil boat (2.5 cm × 1 cm × 0.7 cm) and was melted at 1471° C (80° C superheating) for 1 hour, cooled directly to the desired undercooling, and then treated at that undercooling for the desired time. Care was taken to avoid undershooting the run temperature by setting the temperature about 5° higher than the run temperature and manually resetting the controller as the temperature fell. The time to reach the run temperature was about 8 minutes. The temperature was calibrated against the melting point of diopside using a Pt/Pt–13%Rh thermocouple. At the end of each run, the charge was quenched in air and then transferred into a Thermolyne 1300 electric furnace preheated to about 400° C to release the residual stress in the glass. The charge was held at 400° C for about half an hour and then cooled to room temperature by turning off the furnace. A glass sample for each composition was obtained by direct quenching of the melt from 1471° C followed by the annealing cycle.

Table 1 summarizes the experimental conditions and results. Because several runs at 20° C undercooling and almost all runs at undercoolings larger than 20° C are fully crystallized, only glassy runs at undercoolings of 10° and 20° C were used for SAXS study.

Table 1. List of experimental conditions and results

Run No.	ΔT (°C)	time at ΔT (hrs)	product*	crystal morphology
1. Diopside				
DG		0	g	
D49	10	8	g	
D53		73	g	
D55		116	g	
D58		20	g	
D10	20	168	g	
D12		45	g	
D14		70	g	
D21		27	g	
D30		9	g	
D51	35	5	x	acicular
D52		24	x	acicular
D56		15	g	
D59	50	4	x	spherulitic
2. Diopside + 0.5 wt% TiO_2				
D'G		0	g	
D'51	10	22	g	
D'53		70	g	
D'54		116	g	
D'56		7	g	
D'10	20	20	g	
D'11		6	g	
D'14		43	g	
D'17		12	x	faceted
D'18		21.5	x	faceted
D'19		71	g	
3. Diopside + 1.0 wt% TiO_2				
D"G		0	g	
D"46	10	48	g	
D"51		73	g	
D"57		8	g	
D"58		20	g	
D"8	20	20	x	acicular
D"10		27	g	
D"11		3	g	
D"16		16	g	
D"17		21.5	x	faceted
D"23		52	g	
D"30		9	g	
D"47	35	15	x	acicular
D"59		24	x	acicular

* g: glass; x: fully crystallized.

Our potential difficulty in interpreting the SAXS data is that scattering could occur from gas bubbles in the glass. No bubbles were identified in the several pieces examined by TEM. To affect the SAXS results the bubbles would be too small to be resolved in an optical microscope, although larger ones were looked for and not found.

SAXS analysis

The samples of SAXS study were cut into rectangular slices of about 2 cm × 0.8 cm in area and about 80 μm in thickness and polished on one surface, finishing with 12.5 μm Al_2O_3 powder. Both

the bottom and top of the charge were removed to eliminate crystals nucleated heterogeneously on the surface. The slices were then observed using a disecting microscope to make sure that no bubbles or scratches were present.

The scattering data were collected stepwise at an angular increment of 1.524×10^{-3} degree 2θ over the range from about 0.072 to 0.094 degree 2θ and of 2.54×10^{-3} degree 2θ over the range of 0.094 to 0.102 degree 2θ. A Norelco X-ray generator using Cu$K\alpha$ radiation was operated at 40 kV and 12 mA. The X-ray beam was collimated with a Kratky SAXS camera (entrance slit height: 73 μm, exit slit height: 50 μm) and partially monochromized with a Ni filter and a pulse-height analyzer. The sample was positioned directly behind the collimating system with the polished surface facing the X-ray source, the irradiated area being 0.33 cm^2. The sample-to-detector length was 230 mm. The scattering intensity was recorded with a proportional counter with a digital ratemeter output. Data for the quenched glass sample were always taken on the same day as those for the heat treated glasses of the same composition.

In order to obtain the real scattering of the heat treated samples, the following equation

$$I(\varepsilon) = I_S(\varepsilon) - F\, I_G(\varepsilon) \qquad (7)$$

was applied for data correction (see also Neilson, 1972; Faber and Rindone, 1980). I is the true sample scattering, I_S and I_G the measured heat treated and glass sample scattering, and

$$F = I_{DB}^S / I_{DB}^G, \qquad (8)$$

where I_{DB}^S and I_{DB}^G are the direct beam intensities of heat treated and glass samples taken at zero 2θ at 12 kV and 13 mA. Similar methods of data correction are given by, for example, Williams *et al.* (1965) and Dwiggins (1979). Because our samples are essentially amorphous, data corrections for slit height and slit width were assumed to be negligible (Patel *et al.*, 1972; Schmidt, 1976).

In order to confirm the reproducibility of the data, scattering intensities of one set of samples (diopside + 1.0 wt.% TiO_2, 10° C undercooling) were remeasured under the same operating conditions. The difference of log I values at a given angle is not more than about 2% relative, and that of log (ΔI) for any two angles is of the order of 0.1% relative. These lead to essentially identical Guinier plots and results.
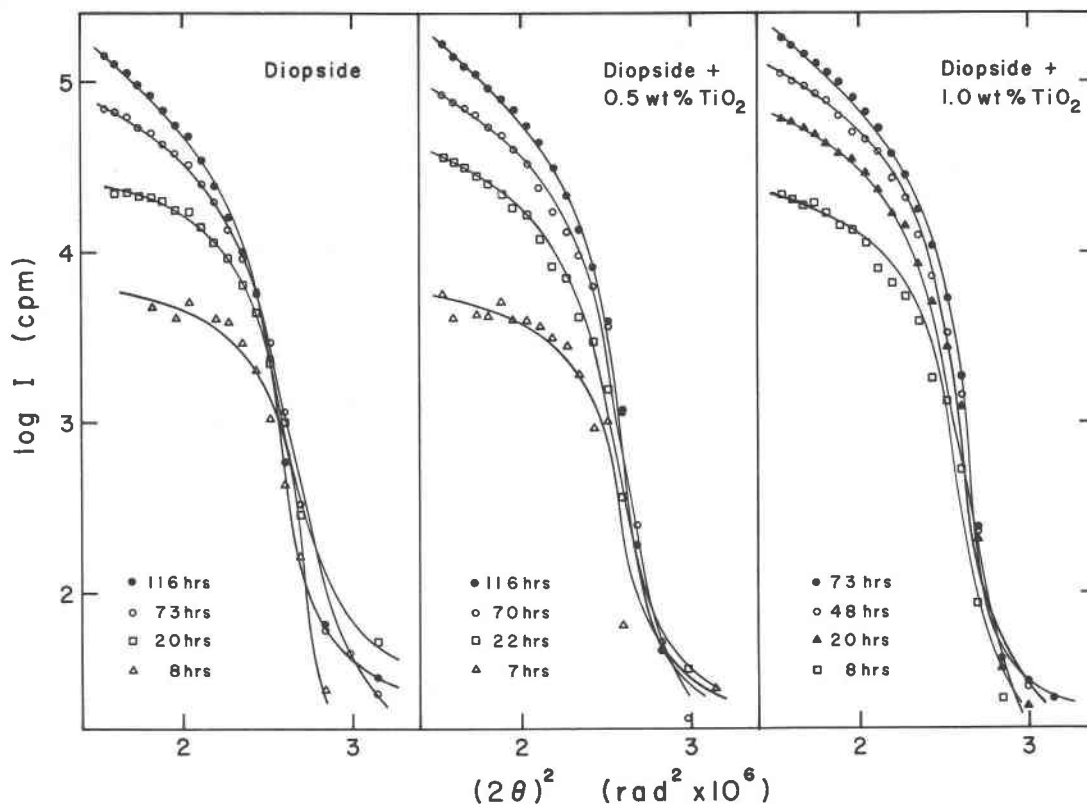
Fig. 1. Guinier plots of heat treated samples at 10° C undercooling. Note the increasing slope at small angles (R_g) and increasing area under the curve (N_p) with increasing time for each composition.

The main purposes of SAXS study are to determine the time dependence of the size and concentration of the subcritical nuclei in the glass. The radius of gyration was found by quadratic fitting of Guinier plots and then evaluating the slope of the nearly linear region in these plots at small angles (Guinier and Fournet, 195; Guinier, 1963; see Figs. 1 and 2). These slopes were used to calculate R_g values using equation (3) and subsequently Q values in equation (5). The determination of $(\Delta\rho)^2$ requires the absolute scattering intensity at zero angle, $I_A(0)$ (Guinier, 1963; Kratky, 1963). Since this intensity is far beyond the detection limit of the counter, values of $I_A(0)$ were obtained by extrapolating $I_S(\varepsilon)$ back to zero and then normalizing with the relationship

$$I_A(0) = I_S(0)/F. \qquad (9)$$

It follows that

$$(\Delta\rho)^2 = I_A(0)/v_p^2. \qquad (10)$$

The value of I_e is $7.9 \times 10^{-26}/cm^2$ (Gerold, 1967). Therefore c and N_p can be calculated using equa-

tions (5) and (6) by assuming that the particles are spherical (see also Hench et al., 1971).

Results

Both raw and corrected scattering data for our samples appear as steeply dome-shaped curves in intensity (I) vs. scattering angle (ε) plots because the data were taken in the tail of the direct beam region and the particles causing scattering are very small in volume. If a relatively larger volume of particles were present, the high scattering intensities should appear at larger angles, out of the direct beam region, resulting in a rather smooth intensity curve covering a larger area in I–ε plot (that is, higher Q value in equation 5). This is the case, for instance, in the work of Hench et al. (1971) and Faber and Rindone (1980), who both studied metastable phase separation in the glasses. The presence of large volumes of particles in their samples was confirmed by TEM study (Faber and Rindone, 1980) and by X-ray diffraction (Hench et al., 1971). Therefore, our corrected data must represent the
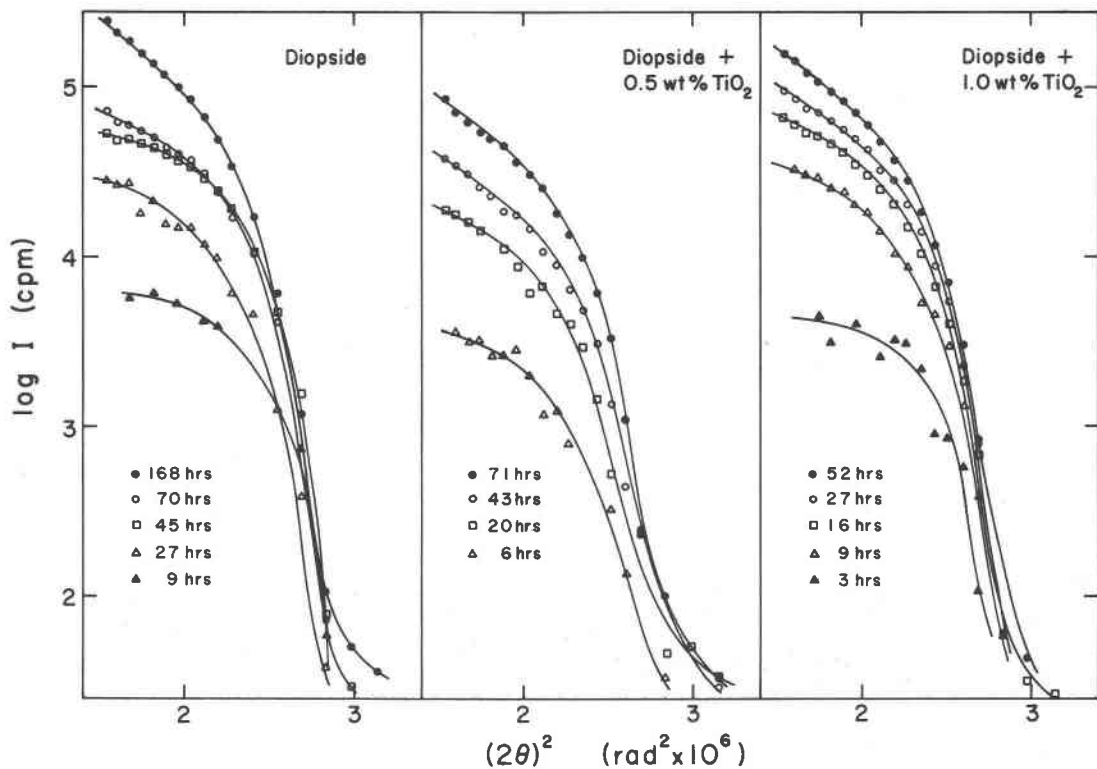
Fig. 2. Guinier plots of heat treated samples at 20° C undercooling. The results are similar to those in Figure 1.

effect of scattering by a small volume of particles in the glass. Because no bubbles are present in the samples, and because the scattering intensities show systematic variation with time (Figs. 1 and 2), these particles are most likely clusters of atoms with radii smaller than the critical radius formed during heat treatment at subliquidus temperatures. Any supercritical nucleus (*i.e.*, those larger than the critical nucleus at a given undercooling), once formed, will grow fast enough to crystallize the whole charge, as evidenced by the high growth rate of diopside (Kirkpatrick *et al.*, 1976) and by our totally crystallized runs.

Size of subcritical nuclei

Table 2 lists the average radius of gyration of subcritical nuclei derived from Guinier plots (Figs. 1 and 2). The values of R_g, ranging from about 200 to 625Å, increase with increasing time for each composition at each undercooling. At a given time and undercooling R_g is larger in the glass with higher TiO_2 content. These data are shown in the plot of R_g^3 (proportional to volume) *vs.* time (Fig. 3). All these plots are characterized by a high and variable slope at short times followed by a period of

lower and constant rate of increase. The slope in the straight line portion is lower at the lower undercoolings and at lower TiO_2 contents and the time required to reach the straight line region is longer at smaller undercoolings and lower TiO_2 content. Figure 4a is a plot of the steady state slope *vs.* TiO_2 content.

Number of subcritical nuclei

The parameters used and the results of the calculation of the volume fraction of subcritical nuclei, c, and the number of subcritical nuclei per unit volume, N_p, are listed in Table 3. Figure 5 shows plots of the calculated number of subcritical nuclei versus time of each undercooling and TiO_2 content. This number increases slowly at shorter times and then more rapidly at longer times. There is some indication that a steady state is approached, although because no nucleation has taken place, this is probably not a true steady state. This behavior is the same as that for the time dependence of ordinary nucleation density (*e.g.*, James, 1974). Therefore, the "steady state" increase rates (I_o' and "induction times" (τ') were evaluated from these plots assuming that the two longest time points fall

Table 2. Average radius of gyration of subcritical nuclei calculated from Guinier plots

starting material	time (hrs)	R_g (Å)
1. $\Delta T = 10°C$		
	116	554.76
Diopside	73	496.35
	20	383.90
	8	230.31
	116	625.76
Diopside + 0.5 wt% TiO₂	70	550.15
	22	458.13
	7	310.27
	73	625.14
Diopside + 1.0 wt% TiO₂	48	574.24
	20	495.82
	8	385.29
2. $\Delta T = 20°C$		
	168	625.15
	70	483.17
Diopside	45	424.71
	27	378.68
	9	266.90
	71	575.00
	43	491.30
Diopside + 0.5 wt% TiO₂	20	396.76
	6	287.50
	52	609.12
	27	499.69
Diopside + 1.0 wt% TiO₂	16	428.00
	9	370.39
	3	268.16

on a straight line. These are presented in Table 4. Figures 4b and 4c illustrate the compositional dependence on the variations of I_0' and τ'. I_0' increases linearly with increasing TiO_2 content, whereas τ'

decreases with increasing TiO_2 content at both undercoolings and may approach a constant, low value at higher TiO_2 content.

Discussion

Cluster radius

The observed increase in the radius of gyration with increasing run time in these experiments is consistent with the traditional physical picture of how the small clusters of atoms which we call subcritical nuclei form. In this picture the clusters are assumed to grow by the addition of single atoms or molecular groups to the surface of the cluster. A melt above its liquidus temperature has few crystal-like clusters and these are small. When the melt is brought to below its liquidus temperature the number and average cluster size begins to increase. Crystals do not appear instantaneously, however, because the free energy of a small cluster is larger than that of the same atoms in the liquid state. In the classical theory this extra energy is assumed to be describable by a surface energy term, although recent work has shown that this is probably inappropriate for small clusters (Hoare, 1979). No matter how it is formulated, this extra energy is a barrier to the formation of crystals, and there is a critical cluster size with a maximum energy which must be exceeded before a cluster can grow into a
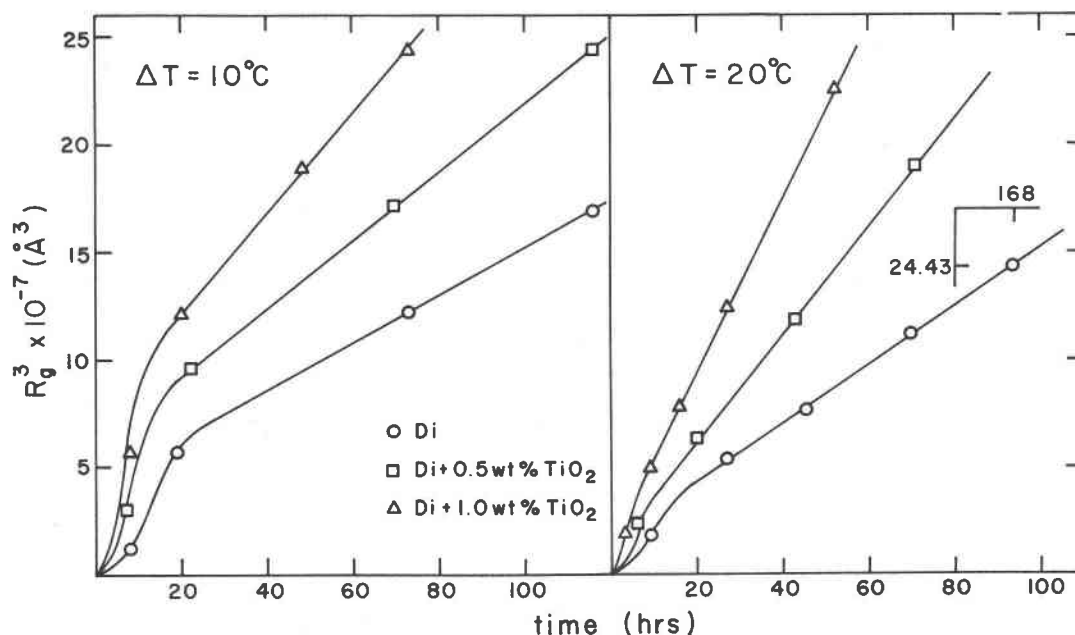

Fig. 3. Change of the radius of gyration of subcritical nuclei as a function of time for all three compositions at 10° C and 20° C undercoolings.
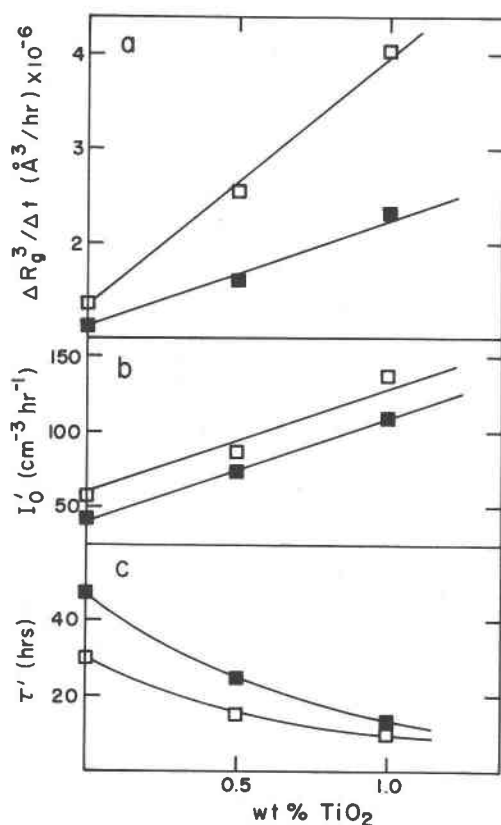
Fig. 4. Variations of $\Delta R_g^3/\Delta t$. I_o' and τ' as a function of TiO_2 content in a diopside melt. Open squares, $\Delta T = 20°$ C, filled squares, $\Delta T = 10°$ C.

crystal. During the time period after the melt is brought below the liquidus temperature subcritical clusters are constantly growing and dissolving. On the average, however, the number and size of the clusters increases with time. Eventually, through a series of fortuitous, random attachments, one cluster exceeds the critical size and begins to grow. With increasing time progressively more crystals nucleate. Eventually a steady state distribution of subcritical clusters is established, and the nucleation rate takes on the steady-state value characteristic of the temperature.

In the experiments described here we have looked at the earliest stages of this process, before any crystals have formed. The increase in R_g, and for that matter the number of clusters, is in good agreement with this picture.

Although the use of surface energy in formulating the barrier to nucleation is probably inappropriate (Hoare, 1979) there must be some energy barrier to crystal formation at small cluster sizes. The rate of

increase in R_g in these experiments is of the order of 3 to 5 angstroms per hour (about 10^{-13} cm sec^{-1}). This is far less than the growth rates for macroscopic crystals from diopside melt, which are of the order of 10^{-3} to 10^{-4} cm sec^{-1} in this undercooling range (Kirkpatrick et al., 1976). Even though R_g represents an average radius, this difference is very large, and can only be due to some free energy barrier preventing the average rate of successful atomic attachment to a subcritical cluster from being as high as it is for a macroscopic crystal.

The data for R_g can be used to estimate the magnitude of this free energy barrier. It is argued above that R_g is weighted towards the largest cluster present. The largest R_g measured before the onset of macroscopic crystal growth is about 625Å. Taking the critical radius to be somewhat larger than this, say 700Å, the extra energy of a cluster in terms of the surface energy can be calculated from the standard relationship:

$$R^* = -\frac{2\sigma}{\Delta G_v} \qquad (11)$$

where R^* is the critical radius, σ is the surface energy, and ΔG_v is the free energy per unit volume driving the reaction (Christian, 1975). ΔG_v can be estimated from the standard relationship

$$\Delta G_v = -\Delta H_f \frac{\Delta T}{T_L} , \qquad (12)$$

where ΔH_f is the latent heat of fusion, ΔT is the undercooling, and T_L is the liquidus temperature. Taking ΔH_f as 34 kcal/mole (Weill et al., 1980), ΔT to be 10°, and T_L to be 1664° K, ΔG is 204 cal/mole. Taking the density of diopside melt to be 2.7 g/cm^3 (Bottinga and Weill, 1970), and its gram formula weight to be 216, ΔG_v is then 2.5 cal/cm^3. Using these values, the extra energy in terms of σ is about 400 erg/cm^2, a value in good agreement with measured crystal-melt surface energies for silicates (no data are available for diopside). This value is at best good to a factor of two and should probably be considered only an order of magnitude estimate. If ΔT were taken to be 20° instead of 10°, σ would be 800 erg/cm^2, and it is not entirely clear that R_g is an accurate measure of the average largest cluster.

Number of clusters

Figure 5, which is a plot of the number of clusters per unit volume vs. time, clearly indicates the non-

Table 3. Parameters used and results of calculations of N_p

starting material	time (hrs)	$n^2 \times 10^{-5}$	$Q \times 10^4$	$(\Delta\rho)^2 \times 10^{-36}$	$V \times 10^3$	θ	$c \times 10^{13}$	$N_p/cm^3 \times 10^{-3}$
1. $\Delta T = 10°C$								
Diopside	116	17.86	6.939	10.17	3.520	0.190	39.13	2.542
	73	5.943	3.199	15.80	3.772	0.169	12.21	1.108
	20	0.908	1.056	74.98	3.101	0.242	0.720	0.142
	8	0.079	0.426	1290	4.023	0.150	0.021	0.019
Diopside + 0.5 wt% TiO_2	116	41.39	11.02	5.783	4.107	0.144	123.6	5.616
	70	9.795	3.872	7.634	3.269	0.214	28.63	2.401
	22	1.853	1.268	31.76	4.443	0.123	2.805	0.323
	7	0.104	0.230	252.7	3.520	0.190	0.052	0.019
Diopside + 1.0 wt% TiO_2	73	41.65	11.22	6.410	4.443	0.123	122.9	5.580
	48	18.17	6.316	7.393	4.275	0.133	57.61	3.375
	20	1.878	1.014	12.51	3.018	0.241	4.278	0.390
	8	0.139	0.159	52.69	4.107	0.144	0.196	0.038
2. $\Delta T = 20°C$								
Diopside	168	47.51	12.80	5.430	4.023	0.150	149.8	6.807
	70	5.161	2.970	17.77	3.267	0.214	13.65	1.342
	45	2.620	2.241	29.83	3.101	0.242	3.919	0.557
	27	0.963	1.167	63.13	3.108	0.231	1.216	0.207
	9	0.060	0.209	489.1	2.934	0.250	0.023	0.013
Diopside + 0.5 wt% TiO_2	71	21.35	7.123	6.921	4.191	0.138	71.48	4.173
	43	6.326	3.512	13.96	4.107	0.144	16.32	1.526
	20	1.039	1.095	48.97	4.275	0.133	1.505	0.267
	6	0.063	0.175	584.2	3.772	0.169	0.031	0.015
Diopside + 1.0 wt% TiO_2	52	35.46	10.32	6.500	4.107	0.144	103.0	5.056
	27	7.650	4.036	13.98	3.940	0.156	18.02	1.601
	16	2.964	2.488	37.01	4.359	0.128	4.626	0.655
	9	1.070	1.386	80.53	3.940	0.156	1.075	0.235
	3	0.072	0.244	457.5	3.101	0.242	0.027	0.016

steady state pre-nucleation behavior of these compositions. As noted above the greater than linear increase in the number of clusters per unit volume is in good agreement with traditional treatments of early stages of transient nucleation.

The most successful theory describing nonsteady state nucleation in silicate compositions is that of Kashchiev (1969) (James, 1974; see Kirkpatrick, 1981, for a brief review), and it appears that this theory also describes our data for subcritical clusters. In Kashchiev's theory the total number of crystals nucleated (in our case the total number of clusters larger than the lower detectability limit) is given by the relationship

$$N_p(t) = I_o \left(t - \frac{\pi^2 \tau}{6} \right), \qquad (13)$$

where I_o is the steady state rate of formation, t is time, and τ is a time constant determined by extrapolating the straight line portion of the data back to zero crystals.

Figure 6 presents our data plotted with Kash-

chiev's predicted relationship, along which all data should lie. The agreement is very good. Because Kashchiev's analysis is based on the classical view that subcritical clusters increase in size and number before nucleation can occur, these data also support the traditional physical picture of the pre-nucleation process.

The present data show that at both undercoolings the number of subcritical nuclei in TiO_2-bearing glasses is greater than the number in TiO_2-free glasses at the same run time. This indicates that

Table 4. Values of "induction time" (τ') and steady state rates of subcritical nuclei increase (I_o') for the three compositions at 10° C and 20° C undercoolings

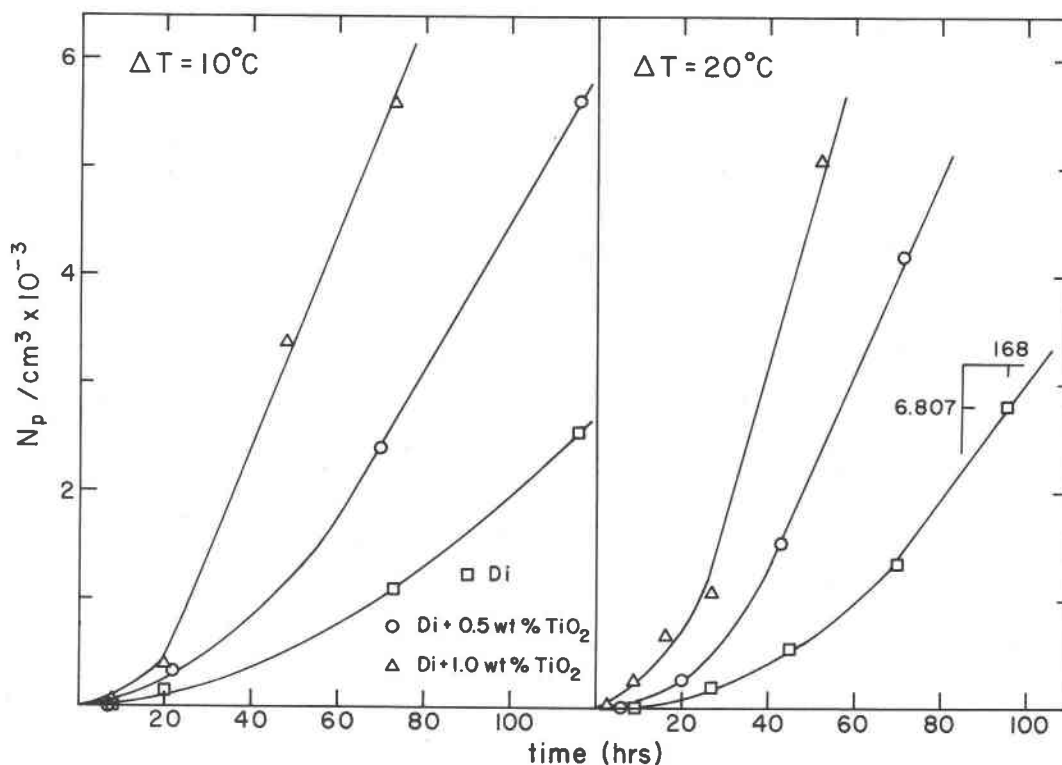| starting material	$\Delta T = 10°C$		$\Delta T = 20°C$	
	τ' (hrs)	I_o' $(cm^{-3}hr^{-1})$	τ' (hrs)	I_o' $(cm^{-3}hr^{-1})$
Diopside	47	42.1	30	57.1
Di + 0.5 wt% TiO_2	25	73.6	15	86.7
Di + 1.0 wt% TiO_2	13	110	10	137

Fig. 5. Calculated number of subcritical nuclei per unit volume as a function of time. Note the greater than linear rate of increase.

cluster formation is significantly aided by the presence of TiO_2 in the melt. Other investigators have also found that TiO_2 aids nucleation. Nikandrov (1964) has investigated the crystallization of a glass with diopside as the liquidus phase, and found that the onset of heterogeneous nucleation takes 8–10 hours at 960° C, whereas for the same glass with 0.01 to 5 wt.% TiO_2 added, nucleation occurs almost instantaneously even at temperatures as high as 1260° C. Leger and Bray (1966) also found that in a glass with a composition close to the anorthite–diopside join the extent of crystallization of these two phases increases with increasing TiO_2 content in the glass. There are several possible explanations for this effect among which it is difficult to choose.

One possible explanation is based on the structural role of TiO_2 (and other polyvalent cations such as Fe^{3+}, Al^{3+}, and P^{5+}) in these melts. Mysen and Virgo (1980) and Mysen et al. (1980) have argued that Ti is 4-coordinated in silicate melts and that the addition of TiO_2 to metasilicate melts (e.g., wollastonite, diopside) results in a decrease in the ratio of non-bridging oxygen to tetrahedrally coordinated cations and thus an increase in chain and sheet units relative to monomers in the melt (i.e., increased polymerization). This effect was also observed by

Kushiro (1975), who found that polyvalent cations cause the equilibrium liquidus fields of more polymerized minerals to expand relative to those of less polymerized minerals. If this is true, it is possible that the increased number of chain-like units allows more rapid formation of clusters with a chain structure.

Another possible effect of TiO_2 in these melts is to decrease the surface energy of the nuclei (Nikandrov, 1964). Assuming constant chemical free ener-
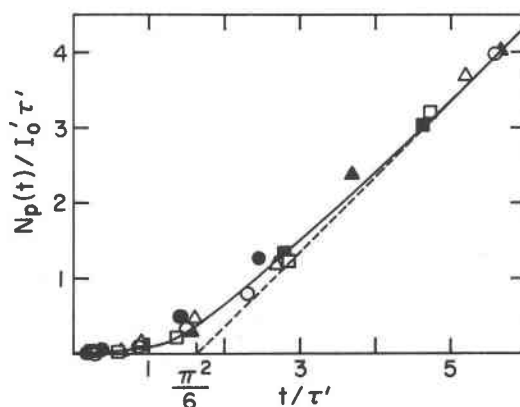

Fig. 6. Comparison of Kashchiev's theory of non-steady state nucleation (solid curve) with experimental data. Open symbols: $\Delta T = 20°$ C, filled symbols: $\Delta T = 10°$ C. Circles: Di; squares: Di + 0.5 wt.% TiO_2; triangles: Di + 1.0 wt.% TiO_2.

gies this will lead to a lower total free energy for a cluster and therefore a more rapid increase in the size and number of clusters in the subcritical region.

It is also possible that TiO_2 itself serves as the center of nucleation (Gutzow *et al.*, 1977). This appears unlikely in the present study because TiO_2 is not a stable phase in our system and has not been detected.

Acknowledgments

References

Bottinga, Y. and Weill, D. F. (1970) Densities of liquid silicate systems calculated from partial molar volumes of oxide components. American Journal of Science, 269, 169–182.

Christian, J. W. (1975) The Theory of Transformations in Metals and Alloys. Pergamon Press, Oxford.

Dwiggins, Jr., C. W. (1979) Absorption correction and normalization of x-ray small angle scattering data for materials producing intense scattering at extremely low angles. Journal of Applied Crystallography, 12, 401–402.

Faber, K. T. and Rindone, G. E. (1980) Small angle X-ray scattering and transmission electron microscopy studies of phase separated soda–lime–silica glasses containing water. Physics and Chemistry of Glasses, 21, 171–177.

Gerold, V. (1967) Application of small-angle X-ray scattering to problems in physical metallurgy and metal physics. In H. Brumberger, Ed., Small-Angle X-ray Scattering, p. 277–317. Gordon and Breach, New York.

Gerold, V. and Kostorz, G. (1978) Small-angle scattering applications to materials science. Journal of Applied Crystallography, 11, 376–404.

Gould, R. W. (1971) Small angle X-ray scattering. In L. L. Hench and R. W. Gould, Eds., Characterization of Ceramics, Chap. 12. Marcel Dekker Inc., New York.

Guinier, A. (1963) X-ray Diffraction, Ch. 10. Freeman, San Francisco.

Guinier, A. and Fournet, G. (1955) Small-Angle Scattering of X-rays. Wiley and Sons, New York.

Gutzow, I., Zlateva, E., Alyakov, S. and Kovatscheva, T. (1977) The kinetics and mechanism of crystallization in enstatite-type glass–ceramic materials. Journal of Materials Science, 12, 1190–1202.

Hench, L. L., Freiman, S. W. and Kinser, D. L. (1971) The early stages of crystallization in a Li_2O–$2SiO_2$ glass. Physics and Chemistry of Glasses, 12, 58–63.

Hoare, M. R. (1979) Structure and dynamics of simple microclusters. In I. Prigogine and S. A. Rice, Eds., Advances in Chemical Physics, v. 40, p. 49–135. Wiley-Interscience, New York.

Hosemann, R., Schönfeld, A. and Wilke, W. (1970) Small angle scattering. In R. Brill and R. Mason, Eds., Advances in Structure Research by Diffraction Methods, v. 3, p. 101–172. Pergamon Press, Oxford, England.

James, P. F. (1974) Kinetics of crystal nucleation in lithium silicate glasses. Physics and Chemistry of Glasses, 15, 95–105.

Kashchiev, D. (1969) Solution of the non-steady state problem in nucleation kinetics. Surface Science, 14, 209–220.

Kirkpatrick, R. J. (1981) Kinetics of crystallization of igneous rocks. In A. C. Lasaga and R. J. Kirkpatrick, Eds., Kinetics of Geochemical Processes, p. 321–398. Mineralogical Society of America, Washington, D.C.

Kirkpatrick, R. J., Robinson, G. R. and Hays, J. F. (1976) Kinetics of crystal growth from silicate melts: anorthite and diopside. Journal of Geophysical Research, 81, 5715–5720.

Kratky, O. (1963) X-ray small angle scattering with substances of biological interest in diluted solutions. In J. A. V. Butler *et al.*, Eds., Progress in Biophysics, v. 13, p. 105–173. Pergamon Press, Oxford, England.

Kushiro, I. (1975) On the nature of silicate melt and its significance in magma genesis: regularities in the shift of the liquidus boundaries involving olivine, pyroxene, and silica minerals. American Journal of Science, 275, 411–431.

Lofgren, G. (1980) Experimental studies on the dynamic crystallization of silicate melts. In R. B. Hargraves, E., Physics of Magmatic Processes, p. 487–551. Princeton University Press, Princeton, New Jersey.

Leger, L. and Bray, J. (1966) An experimental study of the controlled crystallization of alkaline earth silico-aluminate glasses. Glass Technology, 7, 134–142.

Mysen, B. O., Ryerson, F. J. and Virgo, D. (1980) The influence of TiO_2 on the structure and derivative properties of silicate melts. American Mineralogist, 65, 1150–1165.

Mysen, B. O. and Virgo, D. (1980) Trace elements partitioning and melt structure: an experimental study at 1 atm pressure. Geochimica et Cosmochimica Acta, 44, 1917–1930.

Neilson, G. F. (1972) Small-angle X-ray scattering study of complex particle growth in a MgO–Al_2O_3–ZrO_2–SiO_2 glass. Journal of Applied Physics, 43, 3728–3735.

Nikandrov, V. S. (1964) Investigation of the catalyzed crystallization of alkali-free glasses. In E. A. Porai-Koshits, Ed., The Structure of Glasses, v. 3, Catalyzed Crystallization of Glass, p. 188–191. Consultants Bureau, New York.

Patel, I. S., Schmidt, P. W. and Ohlberg, S. M. (1972) Small-angle scattering study of phase separation in glasses. Journal of Applied Physics, 43, 1636–1641.

Schmidt, P. W. (1976) Collimation corrections in small angle x-ray and neutron scattering. In F. R. Ahmed *et al.*, Eds., Crystallographic Computing Techniques, p. 363–375. Munksgaard, Copenhagen, Denmark.

Weill, D. F., Hon, R. and Navrotsky, A. (1980) The igneous system $CaMgSi_2O_6$–$CaAl_2Si_2O$–$NaAlSi_3O_8$: variations on a classic theme by Bowen. In R. B. Hargraves, Ed., Physics of Magmatic Processes, p. 49–92. Princeton Unviersity Press, Princeton, New Jersey.

Williams, J. A., Phillips, B., Rindone, G. E. and McKinstry, H. A. (1965) Small-angle X-ray scattering by metastable liquid immiscibility in glass. In W. M. Mueller *et al.*, Eds., Advances in X-ray Analysis, v. 8, p. 59–77. Plenum Press, New York.